






# An Optimal Operation Strategy for Collaborative Flexibility Provision of a Carbon Capture and Utilization Process with Wind Energy

Arash E. Samani , *Student Member, IEEE*, Nezmin Kayedpour , *Student Member, IEEE*, Farjam Kayedpour, Jeroen D. M. De Kooning , *Senior Member, IEEE*, Guillaume Crevecoeur  and Lieven Vandeveldel , *Senior Member, IEEE*

**Abstract**—Improving power system flexibility by responsive demand is essential for integrating wind energy with a high level of variability in power systems. Carbon dioxide-based chemical processes as energy-intensive industrial loads may offer a vast potential of new forms of flexible operation due to their existing control infrastructure and storage capabilities. However, a collaborative decision model is needed for optimal energy sharing among the chemical plant and the grid under the variations and uncertainties of wind power. This study develops an optimal two-stage stochastic programming model for a novel flexible operation strategy of the chemical process coupled with wind turbines. In the proposed control scheme, a small-scale wind farm provides the power input of a chemical plant. Wind turbines are connected to the grid and actively participate in the day-ahead energy and reserve markets, considering the chemical plant as a source of flexibility. An equivalent scenario-based model of the proposed optimization problem is suggested using the Group Method of Data Handling (GMDH) for a data-driven prediction of stochastic variables. Simulation results demonstrate the effectiveness and significance of the proposed approach for an optimal and collaborative contribution in ancillary market of a carbon dioxide-based chemical plant supplied by wind energy.

**Index Terms**—Wind energy, Carbon dioxide-based chemical plant, Optimization, Flexible operation, Day-ahead market.

## NOMENCLATURE

$\alpha$	Additional incentive component
$\bar{f}_e$	Average grid frequency for quarter-hourly basis
$\Delta f$	Grid frequency deviation
$\dot{m}$	Mass flow rate
$\eta_c$	Converter efficiency
$\eta_g$	Generator efficiency
$\mathbb{E}_\omega$	Expected value for each scenario
$\lambda_e^{\text{sch}}$	Revenue for scheduled power injection to the grid
$\lambda_r^{\text{sch}}$	Revenue for scheduled reserve power
$\lambda_{\Delta e}^+$	Revenue for positive deviation in power injection
$\lambda_{\Delta e}^-$	Penalty for negative deviation in power injection

$\lambda_{\Delta r}^+$	Revenue for positive power reserve deviation
$\lambda_{\Delta r}^-$	Penalty for negative power reserve deviation
$\lambda_{\Delta r}^M$	Monthly remuneration for power reserve provision
$\omega$	Wind scenario
$\Omega_c$	Compressor rotor speed
$\Omega_m$	Motor rotor speed
$\phi$	Ratio between $\dot{m}_{\text{CO}_2}$ and $\dot{m}_{\text{H}_2}$
$\phi_{\text{ref}}$	Reference ratio between $\dot{m}_{\text{CO}_2}$ and $\dot{m}_{\text{H}_2}$
$\rho$	Air density
$\tau_m$	Motor torque
$C_d$	Double layer capacitance
$C_p$	Wind turbine power coefficient
$C_p^{\text{Max}}$	Wind turbine maximum power coefficient
$e(t)$	Electrical potential source
$f_e$	Grid frequency
$g$	Function of formic acid production
$K$	Droop constant
$P$	PEM electrolyzer power consumption
$P_e(\omega)$	Injected electrical power in each wind scenario
$P_e^{\text{sch}}$	Scheduled electrical power in a day-ahead market
$P_{\text{Fa}}^{\text{Max}}$	Maximum allowable formic acid relative power
$P_{\text{Fa}}^{\text{Min}}$	Minimum allowable formic acid relative power
$P_{\text{Fa}}^{\text{OPr}}$	Operational formic acid power
$P_g(\omega)$	Total injected power to the grid
$P_i$	Input pressure
$P_o$	Output pressure
$P_{\text{ref}}$	PEM electrolyzer reference power
$P_r(\omega)$	Activated power reserve in each wind scenario
$P_r^{\text{sch}}$	Scheduled power reserve in a day-ahead market
$P_r^+(\omega)$	FCR upward regulation in each wind scenario
$P_r^-(\omega)$	FCR downward regulation in each wind scenario
$P_{\text{wt}}$	Wind turbine electrical power
$P_\omega$	Total available power in each wind scenario
$p_{\text{Fa}}(\omega)$	Formic acid relative power in each wind scenario
$R$	Blade radius
$R_d$	Solution resistance
$R_m$	Electrolyte resistance
$T_i$	Input temperature
$T_o$	Output temperature
$v_w$	Wind speed
$v_w^{\text{ci}}$	Cut-in wind speed
$v_w^{\text{cu}}$	Cut-out wind speed
$v_w^{\text{n}}$	Nominal wind speed
$Z$	Total income in the proposed strategy
$Z_b$	Total income in the baseline strategy

A. E. Samani, N. Kayedpour, J. D. M. De Kooning, G. Crevecoeur and L. Vandeveldel are with the Department of Electromechanical, Systems & Metal Engineering, Ghent University, Tech Lane Ghent Science Park - Campus Ardoyen, Technologiepark-Zwijnaarde 131, B-9052 Ghent, Belgium. A. E. Samani, N. Kayedpour, J. D. M. De Kooning, G. Crevecoeur and L. Vandeveldel are also with FlandersMake@UGent - Corelab MIRO. F. Kayedpour is with the Department of Industrial Management, Management and Accounting Faculty, Allameh Tabatabai University, Tehran, Iran. (email: ebnealisamani.arash@ugent.be; nezmin.kayedpour@ugent.be; Kayedpour921@atu.ac.ir; jeroen.dekooning@ugent.be; guillaume.crevecoeur@ugent.be; and lieven.vandeveldel@ugent.be).

## I. INTRODUCTION

**T**HE global energy consumption has dramatically increased since the industrial revolution. During the nineteenth century, the excessive use of fossil fuels such as coal, natural gas, and oil has significantly added an extreme amount of carbon dioxide and other greenhouse gases to the atmosphere. The excessive emission of carbon dioxide subsequently results in global warming and other severe environmental problems. The Paris Agreement global framework for avoiding climate change has set out targets to minimize carbon dioxide emission [1]. The European Union (EU) has also conducted a schedule for Europe's neutral climate till 2050 by supporting the sustainable expansion of renewable energy and Carbon Capture and Utilization (CCU) technologies. This policy makes Europe a global leader in tracking the record of decarbonizing power systems [2]. Currently, wind energy has the most extensive contribution to the EU's renewable energy production and is responsible for providing up to 759 TWh by 2030, which will be 23% of the total electricity request [3]. The EU has decided to reduce its net greenhouse gas emissions by at least 55% by the end of this decade before eventually attaining net-zero by 2050 [4]. The EU's regulations ensure the development of technologies that make it possible to integrate the energy produced from renewable sources into CCU-based processes.

CCU processes require access to  $H_2$  as a raw material to synthesize added value chemicals such as polyols, polyurethane, formic acid, methane, and methanol [5], [6].  $H_2$  can be obtained from water electrolysis or biomass gasification using electricity sources. However, electrolysis has a significant electricity consumption rate in these processes, known as an indication of high operating costs. Thus, it is highly recommended for CCU processes to have access to low-cost renewable energy to significantly decrease their costs and increase market competitiveness, considering both environmental and economic points of view [7], [8]. Many studies have considered opportunities for integrating CCU processes with renewable energy sources [7], [9]–[11]. [12] used methanol production via carbon dioxide hydrogenation as a case study to conceptually analyze the flexibility of chemical processes that can operate with a varying load, while meeting a reliable production target. This study reveals evident potential advantages of process flexibility under a high penetration level of renewable energy. Although chemical processes conventionally prefer to operate at a steady-state with a constant load, combining variable renewable energy can be addressed by optimal coordination between flexible energy generation and flexible chemical production [13], [14].

Coupling CCU processes with variable renewable sources is an efficient path to decrease greenhouse gas emission rates. However, few studies look into the potential role of these sources in power system flexibility and demand response. Nevertheless, integrating CCU processes with renewables can be complementary with energy storage devices for surplus electricity generation and even an adequate resolution to provide grid balancing services. In [15], a case study for the UK and Spain is presented to use methanol and hydrogen

as chemical storage compounds for wind and solar energy. The study used nonlinear programming to solve a trade-off between investment and production capacity. In [16], an optimal integration of renewable-based processes for several products is studied. However, no proposal with a relevant business model and actual power market operation is reported in this study. In [17], a flexible operation strategy is proposed for formic acid synthesis providing FCR in smart grids. In [18], the requirements needed for an environmentally and economically viable methanol producing carbon dioxide utilization process explored for participating in the energy system with consideration of the day-ahead or intraday bidding system, including the seasonality of wind.

The flexibility of the power system has become essential with an evolving electricity market landscape to cancel the effects of uncertainties and variabilities that are evident due to the increased penetration of renewable energy in the energy mix [19], [20]. Therefore, a collaborative energy-sharing strategy is required for CCU processes coupled with renewables to actively participate in the ancillary services such that the power system can accommodate even the most extensive deviation range of uncertainties. This solution can significantly accelerate the integration of intermittent electricity sources, assist demand flexibility, and decrease the dependence on renewables support schemes [21].

Although little attention is shown to the capacity of CCU processes coupled with renewables in demand response and grid balancing services, several studies suggest a collaborative energy-sharing optimization model among other responsive demands with flexible operation, the power grid and renewable energy. [22] proposed a controlled electric vehicle charging strategy to optimize the peak-valley difference of the grid, considering the regional wind and photovoltaic (PV) power outputs using probabilistic models. In [23], a stochastic model based on chance constraints is suggested for network congestion management in the day-ahead power market with consideration of the uncertainty of wind power and demand-side response in order to determine the optimal daily dispatch of generators and loads, and to minimize the risk of transmission congestion. In [24], a two-stage energy sharing framework is proposed for a new prosumer microgrid with renewable energy generation, multiple storage units, and load shifting. The proposed robust energy sharing schedule reveals the potential to overcome the uncertainties of market prices and renewable energy.

The main contribution of this study is an optimal collaborative strategy for the flexible operation of a carbon dioxide-based chemical process synthesizing formic acid connected to a wind energy source that actively participates in the day-ahead energy and reserve markets. The significance of the energy sharing concept in the proposed arrangement is explored in which wind turbines can support the power grid while delivering the energy consumption of the process based on economic viability and the plant owners' willingness under different scenarios and system actions. The total profit is maximized by an optimal contribution of the wind power in the electricity/reserve market and/or by producing formic acid. Maximization of profit as the optimization criterion resolves

the bidding strategy that should be set before the day-ahead market's closure. Therefore, a two-stage stochastic optimization framework is suggested, considering the likelihood of different scenarios of wind power and grid demand for the day ahead. Thus, the chemical plant base-load can be decided while (1) maximizing the share of electricity/reserve offering to the market, considering stochastic behavior of wind and grid frequency in a day ahead, and (2) maximizing the formic acid production and CO<sub>2</sub> capture, guaranteeing the profitability of the process and the decarbonization policy. The behavior of the process subsystems with fast dynamics, i.e., the electrolyzer and compressors, are investigated up to the reactor inlet for the proposed optimal energy-sharing framework in varying operating conditions. The dynamic performance of the reactor is not included in this study since the reactor's dynamic for such liquid phase reactions is sufficiently slow (minutes to hour scale) [25]. Also, the residence time can be longer than the power-consuming subsystems responding to frequency changes in below 10 s for the provision of Frequency Containment Reserve (FCR). Therefore, such variations are assumed to be absorbed and dampened due to the reactor's slow dynamics, similar to the systems discussed in [26] with having time constants on the order of minutes to hours. Nevertheless, variations on the hour scale, which are not in the scope of this study, are typically compensated by a compressed storage tank.

The article is structured as follows: Section II introduces the wind turbine and chemical plant models. Section III formulates the methodology and optimization problem based on wind and grid frequency prediction. Section IV provides an overview of the outcomes and results, while Section V presents a discussion and conclusions.

## II. SYSTEM DESCRIPTION

This section describes and illustrates the wind turbine model and the design of the flexible CCU-based chemical process. Fig. 1 gives a general overview of the system under study. Wind power is allocated close to the chemical process, which captures carbon dioxide and produces formic acid. The system is also connected to the power grid and can deliver ancillary services for grid balancing. The chemical plant's base-load and the share of FCR [27] should be determined based on the available wind power, electricity/reserve prices and the marginal profit of formic acid production, taking into account the variability of wind energy and grid frequency

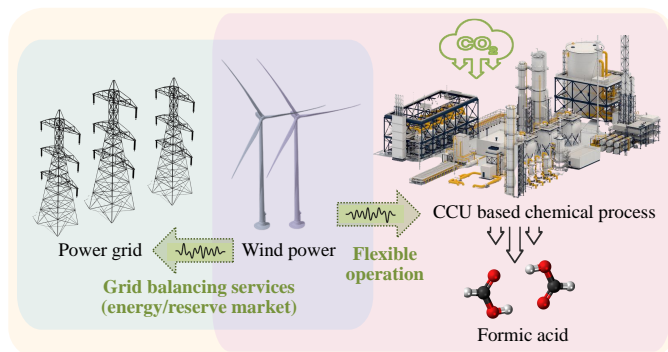
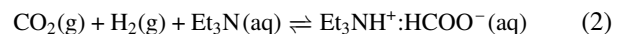


Figure 1: Overview of the hybrid system.

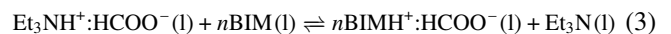
within a scenario-based stochastic framework. In what follows, the system component models will be described in more details. These models will be used to validate the proposed optimization strategy under different operational conditions.

### A. Chemical plant model

The chemical process under study produces formic acid by thermo-catalysis through hydrogenation of CO<sub>2</sub> over heterogenised ruthenium catalysts. Formic acid is a basic chemical that finds use in a variety of applications such as leather and rubber production, textiles, pharmaceuticals, preservatives and antibacterial agents in livestock feed. Highly concentrated CO<sub>2</sub> can be captured from various sources, e.g., fossil fuel power plants or bio-refineries. The price per tonne can be nearly free, or even negative with incentives, or can rise up to 600 €/tonne for direct air capture [28]. This study assumes that the captured CO<sub>2</sub> is available under ambient conditions and has a negligible impact on the Net Present Value (NPV), which is more affected by consumables, formic acid production and electricity consumption. Therefore, CO<sub>2</sub> availability is not supposed to constrain the economic optimality and limit the performance of the proposed flexible control architecture. Fig. 2 shows the process flow diagram for conversion of CO<sub>2</sub> and H<sub>2</sub> to formic acid based on the process developed in [29]. The synthesis process comprises five sections: (I) the compression stage of H<sub>2</sub> and CO<sub>2</sub>, (II) the reaction stage, (III) the formic acid enrichment stage to concentrate the reactor product, (IV) the amine exchange stage and (V) the distillation stage for formic acid formation and purification. The process uses 2464 kg/h of CO<sub>2</sub> and 112 kg/h of H<sub>2</sub> to produce 10 kt/yr of formic acid. In this model, it is assumed that the captured CO<sub>2</sub> is available at atmospheric pressure. Therefore, a compression stage is required to increase the pressure up to the optimal operating pressure of the reactor. The required H<sub>2</sub> is supplied by a 5.79 MW Polymer Electrolyte Membrane (PEM) electrolyser. The CO<sub>2</sub> and H<sub>2</sub> are pressurized before feeding into the reactor. In the reaction stage, CO<sub>2</sub> is hydrogenated in the presence of triethylamine (Et<sub>3</sub>N) to drive the thermodynamically limited equilibrium of the hydrogenation via the formation of a stable adduct, Et<sub>3</sub>NH<sup>+</sup>:HCOO<sup>-</sup> [30]:



The liquid stream from the catalytic reactor is fed into the evaporator to concentrate the Et<sub>3</sub>NH<sup>+</sup>:HCOO<sup>-</sup> adduct at an Acid to Amine Ratio (AAR) of 2.3 by removing water and excess triethylamine, which allows the amine exchange in the next stage. Since the Et<sub>3</sub>NH<sup>+</sup>:HCOO<sup>-</sup> adduct can not be directly separated into formic acid and triethylamine, the concentrated Et<sub>3</sub>NH<sup>+</sup>:HCOO<sup>-</sup> is combined with *n*-butyl imidazole (*n*BIM) to form *n*BIMH<sup>+</sup>:HCOO<sup>-</sup> [31]. Then, the product is introduced into a separation column to produce pure formic acid according to reactions (3) and (4):



A dynamic model of the chemical process is developed to represent the process dynamics under flexible operation. In this

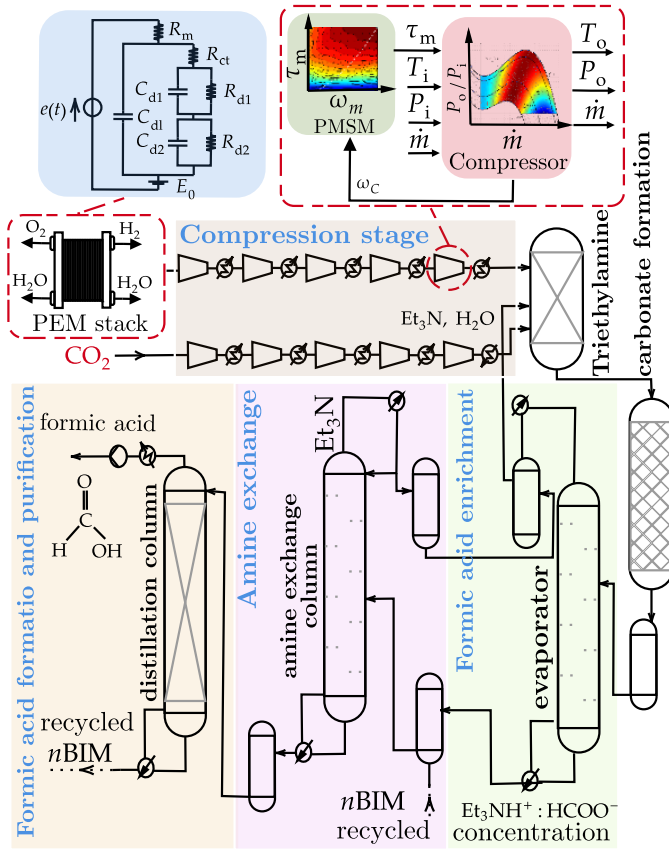


Figure 2: Process flow diagram.

process, the PEM electrolyser and compression stages are selected as the main electrical components to provide flexibility due to their fast dynamic response and significant power consumption. Therefore, the dynamic model is developed based on the fast dynamic response of the PEM electrolyser and the compressors, while monitoring the impact on the subsequent stages. The process elements are individually modelled in Matlab/Simulink. Then they are integrated to build a complete model of the synthesis process. A Randles-Warburg (RW) impedance equivalent is used to model the electrochemical dynamics of the PEM electrolyser.

Hydrogen and carbon dioxide input streams are pressurized in two separate compression stages to reach the reactor pressure of 120 bar. The compression stages are first modelled in Aspen HYSYS to determine the required specifications to reach the desired pressure level at the reactor, i.e., the number of stages and the size of the compressors. Then, the compressors are modelled based on the acquired data, and they are coupled with models of Permanent Magnet Synchronous Motors (PMSM) with a variable speed drive to enable the compressors to operate at variable speeds. The dynamic model of the PMSMs is developed in the rotating  $d-q$  synchronous reference frame, including copper losses, iron losses and armature reaction effects [32]. The compressors are modelled based on the compressor's mechanical dynamics using the first-order equation of motion, including rotational inertia and the compressor and motor torques. The variable-speed operation is performed by regulating the motor torque by using field-oriented control, and the corresponding output pressure

and temperature at each rotational speed is obtained by using an approximation of the compressor performance map. The reactor model is developed based on the data available in [29], assuming a constant ratio of  $\text{CO}_2$  and  $\text{H}_2$  at the reactor. Based on the developed model, the formic acid production is obtained as a function of the relative power consumption of the process  $g(p_{\text{Fa}}(\omega))$ :

$$g(p_{\text{Fa}}(\omega)) = -31.79 \cdot p_{\text{Fa}}(\omega)^2 + 433.16 \cdot p_{\text{Fa}}(\omega) - 61.97 \quad (5)$$

where  $p_{\text{Fa}} = P_{\text{Fa}}^{\text{opr}}/P_{\text{Fa}}^{\text{max}}$  is the relative power calculated based on operating formic acid power consumption  $P_{\text{Fa}}^{\text{opr}}$  and maximum formic acid power consumption  $P_{\text{Fa}}^{\text{max}}$ , where  $p_{\text{Fa}} \in [0, 1]$ . The numerical value of the formic acid production  $g$  is also expressed in kg/h.

The piecewise linearization of (5) results in:

$$g(p_{\text{Fa}}(\omega)) = \begin{cases} 368.65 \cdot p_{\text{Fa}}(\omega) - 35.28, & \text{if } 0.57 \leq p_{\text{Fa}}(\omega) < 1.44 \\ 313.50 \cdot p_{\text{Fa}}(\omega) + 44.54, & \text{if } 1.44 \leq p_{\text{Fa}}(\omega) < 2.31 \\ 258.35 \cdot p_{\text{Fa}}(\omega) + 172.27, & \text{if } 2.31 \leq p_{\text{Fa}}(\omega) < 3.18 \\ 203.01 \cdot p_{\text{Fa}}(\omega) + 348.50, & \text{if } 3.18 \leq p_{\text{Fa}}(\omega) < 4.05 \\ 147.82 \cdot p_{\text{Fa}}(\omega) + 527.18, & \text{if } 4.05 \leq p_{\text{Fa}}(\omega) < 4.92 \\ 92.75 \cdot p_{\text{Fa}}(\omega) + 843.21, & \text{if } 4.92 \leq p_{\text{Fa}}(\omega) < 5.79 \end{cases} \quad (6)$$

In order to facilitate the collaborative operation of the CCU based process with wind energy, a control design is needed to enhance the process flexibly at the operational level. However, there are a few concerns regarding the dynamic modeling of the process. In [33], dynamic modeling of methanation reactors is studied during start-up (transient) and regulation in intermittent power-to-gas applications. It has been discussed that when the methanation unit is fed with a fraction of inlet flow (partial load), the temperature evolves towards the new steady state. In order to enhance the flexible operation of the system, avoiding a hot spot through the catalytic bed,  $\dot{m}_{\text{CO}_2}$  staging should be adjusted with respect to the initial full load design, which means part of carbon dioxide should bypass the first and second reactor. The methanation unit can thus operate safely between 45% and 100% of the nominal load. Moreover, the experimental results presented in [34] show how a full-scale methanation reactor can be operated under variable process conditions for 1000 hours without complications. The start and stop can be performed within minutes, considering the temperature profile. Therefore, overheating should not be a concern in such processes. In [35], a thorough review is presented dedicated to feasible applications of formic acid production by thermo-catalysis through hydrogenation of  $\text{CO}_2$  over heterogenized ruthenium catalysts using low-carbon renewable electricity, considering the dynamic behavior of the entire chemical process. However, the main contribution of this research is to suggest using the previously-studied flexibility of such a process in the provision of FCR [26], where the electrical flexibility is mainly determined by, e.g., the electrolysis and compressors. Therefore, the proposed control architecture is designed to enhance the process flexibly at the operational level. The control system is able to track the reference power while maintaining the process efficiency at the

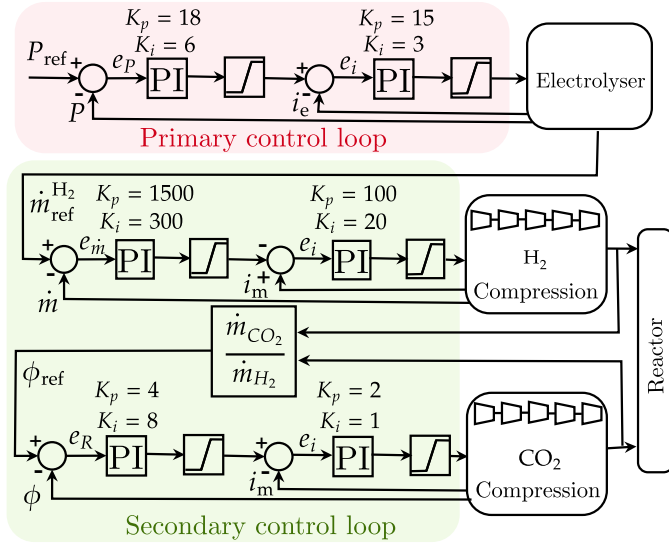


Figure 3: Control system for flexible operation of the PEM electrolyser and the CO<sub>2</sub> and H<sub>2</sub> compression stages.

desired level with respect to the system's physical limitations. The generated hydrogen mass flow rate at the process input  $\dot{m}_{H_2}$  changes due to the varying power setpoint for FCR provision. Thus, the compressors' rotational speeds need to be regulated based on the H<sub>2</sub> production variations. Otherwise, the safe and optimal operating condition of the reactor will be violated. Fig. 3 illustrates the proposed control scheme for flexible operation of the process. The primary control loop tracks the power reference signal  $P_{ref}$  by regulating the PEM electrolyser power consumption  $P$ . The secondary control loop follows the primary controller. It tracks the reference signal  $\phi_{ref}$ , which maintains the desired ratio of the hydrogen mass flow rate  $\dot{m}_{H_2}$  and the carbon dioxide mass flow rate  $\dot{m}_{CO_2}$  at the reaction stage. The control architecture enables the compressors to operate at different rotational speeds by regulating the PMSM torque using field-oriented control.

The process model employed here can be considered semi-dynamic in the sense that the components with a short time constant and direct impact on electric power, i.e., electrolysis and compressors, are represented by a fully dynamic model, e.g., by means of Randles-Warburg equivalent cells for the electrolyzer and rotating reference frame models and motion equations for the compressors. The reactor itself is modeled quasi-statically. The above models are presented with more details in [17]. This semi-dynamic modeling approach is justified since the electrical flexibility is mainly provided by the electrolyzer and compressors, while a continuous reactor can operate with a considerably higher residence time [25]. Moreover, [26] proposed that slow systems with a high time constant in the order of minutes can effectively dampen and absorb the higher frequency dynamics of the flexible provision of ancillary services. The research here focuses on FCR, which requires a fast response (second scale) on the grid side, for which the time constant of the electrolysis and compressors are well suited. It is also important to note that the quadratic functions 5 and piece-wised 6 are only used in the stochastic programming framework, where the optimal decision should

be taken hourly based on day-ahead prediction, considering the penalty and remuneration system on a quarter-hourly basis. Therefore, 5 and 6 estimate the formic acid production as a function of electrical power consumption in a steady-state way.

### B. Wind turbine model

The wind energy source in this article consists of two NREL 5MW wind turbines [36]. The NREL 5MW baseline wind turbine model is implemented and coupled to a generator and converter model. The generator is a direct-drive PMSG, which is modeled with an equivalent scheme in the rotating reference frame, as presented in [32]. The efficiency curve is included in the model as a function of different operating points [37]. As shown in Fig. 4, the wind turbine operating mode depends on the wind speed. Three operating regions can be defined. In the partial load region, where the wind speed is below the rated value, the pitch angle is kept in an optimal position, and the generator-torque controller aims to maximize power capture by means of Maximum Power Point Tracking (MPPT). The transition zone can be considered as an extension of the first zone. In this region, the primary objective is to regulate generator speed at rated power by using pitch control. The blade-pitch controller aims to regulate the generator speed at its rated value in the full load region, where the wind speed is above the rated value. Proportional integral (PI) controllers are used for the pitch and torque control systems. The used control system is discussed in more detail in [38], [39]. The total electrical power obtained from each wind turbine can be expressed as:

$$P_{wt} = \begin{cases} 0 & , v_w < v_w^{ci} \\ \frac{1}{2} \rho \pi R^2 v_w^3 \eta_g \eta_c C_P^{\max}(\lambda_{opt}, \theta_{opt}) & , v_w^{ci} \leq v_w \leq v_w^n \\ \frac{1}{2} \rho \pi R^2 v_w^3 \eta_g \eta_c C_P(\lambda, \theta) & , v_w^n \leq v_w \leq v_w^{cu} \end{cases} \quad (7)$$

where  $\rho$  is the air density in kg/m<sup>3</sup>,  $R$  indicates the blade length in m, the wind speed is denoted by  $v_w$  in m/s.  $C_P$  is the power coefficient as a function of the dimensionless tip speed ratio  $\lambda$  and the blade pitch angle  $\theta$  in degrees. The generator and converter efficiency are characterized by  $\eta_g$  and  $\eta_c$ , respectively, which vary depending on the operating point.

In order to obtain the realistic power curve of the wind turbine, the turbine is operated under different wind conditions,

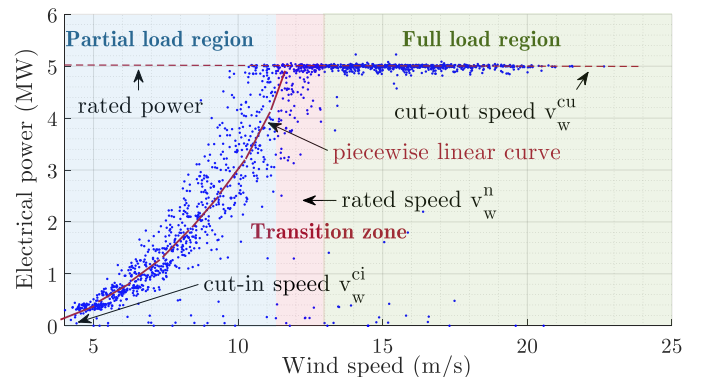


Figure 4: 5MW wind turbine power curve.

i.e., mean wind speed and turbulent intensity, and the power out put of the wind turbine is measured. The data points are obtained from 20 simulations over 200 minutes for mean wind speeds of 5 to 20 m/s and turbulence intensity of 10 to 20%. After data preprocessing and eliminating the outliers that exist due to turbulence, a cubic polynomial curve fitting is used to fit the wind turbine power curve, which can be defined as:

$$P_{wt} = \begin{cases} 0 & , 0 < v_w < v_w^{ci} \\ a v_w^3 + b v_w^2 + c v_w + d & , v_w^{ci} \leq v_w \leq v_w^n \\ 5 & , v_w^n \leq v_w \leq v_w^{cu} \end{cases} \quad (8)$$

where  $v_w^{ci}$ ,  $v_w^{cu}$  and  $v_w^n$  are respectively the cut-in, cut-out and rated wind speeds in m/s.  $P_{wt}$  is a wind turbine electrical power in MW.  $a$ ,  $b$ ,  $c$  and  $d$  are the parameters of a cubic polynomial fitted to the data. The parameter values are:

$$\begin{aligned} v_w^{ci} &= 3, & v_w^n &= 11.9, & v_w^{cu} &= 25 \\ a &= 0.0019, & b &= 0.0227, & c &= -0.1140, & d &= 0.1359 \end{aligned} \quad (9)$$

A piecewise linearization is employed to divide the nonlinear function of two wind turbines into several linear sections as follows:

$$P_{wt} = \begin{cases} 0 & \text{if } v_w < v_w^{ci} \\ 0.1152 \cdot v_w - 0.2961 & \text{if } v_w^{ci} \leq v_w < 4 \\ 0.2062 \cdot v_w - 0.6601 & \text{if } 4 \leq v_w < 5 \\ 0.3086 \cdot v_w - 1.1721 & \text{if } 5 \leq v_w < 6 \\ 0.4224 \cdot v_w - 1.8549 & \text{if } 6 \leq v_w < 7 \\ 0.5476 \cdot v_w - 2.7313 & \text{if } 7 \leq v_w < 8 \\ 0.6842 \cdot v_w - 3.8241 & \text{if } 8 \leq v_w < 9 \\ 0.8322 \cdot v_w - 5.1561 & \text{if } 9 \leq v_w < 10 \\ 0.9916 \cdot v_w - 6.7500 & \text{if } 10 \leq v_w < 11 \\ 0.8425 \cdot v_w - 5.1100 & \text{if } 11 \leq v_w < v_w^n \\ 5 & \text{if } v_w^n \leq v_w \leq v_w^{cu} \end{cases} \quad (10)$$

### III. OPTIMIZATION PROBLEM FORMULATION

The decision-making of the proposed stochastic optimization framework consists of two objectives. The first objective is to determine the strategic bidding for the scheduled electricity and reserve quantity in the day-ahead market at the market-clearing price and in a non-price-making position. The second objective is to optimize the formic acid production the next day, satisfying the scheduled bidding quantities as much as is feasible. Once the participant decides the bidding quantity, it will not be allowed to change its decision on the next day against the signed corresponding transaction agreement. Therefore, a two-stage stochastic optimization process is formulated to support decision-making during the different stages and periods. The two-stage stochastic energy sharing model allows the participant to make an optimal decision considering the day-ahead electricity and reserve transactions (in the first stage) while optimizing tomorrow's real-time chemical plant operations (in the second stage). When tomorrow comes the deviation from the promised quantities will be compensated by the chemical plant upward or downward activations. The central assumption is that the decision-maker can estimate the expected value of possible scenarios related to wind speed

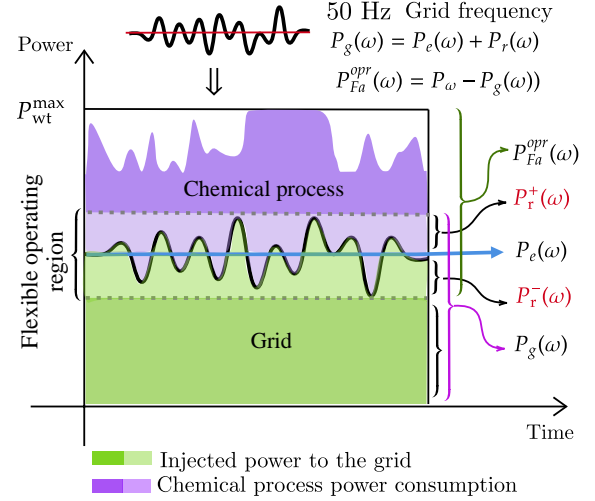


Figure 5: Collaborative strategy for energy sharing.

and grid frequency when offering its bidding quantity in the day-ahead electricity/reserve market. On the next day, the decision-maker then optimizes the base-load of formic acid production based on available wind power and grid frequency. Fig. 5 shows the collaborative strategy for energy sharing among formic acid production  $P_{Fa}^{opr}(\omega)$ , and the power injected into the grid  $P_g(\omega)$ . This includes both electricity  $P_e(\omega)$  and reserve quantities for upward  $P_r^+(\omega)$  and downward  $P_r^-(\omega)$  regulation. As the flexible operation region illustrates in Fig. 5, the available reserve margin can be allocated to both formic acid production and the electricity market based on grid frequency and the Transmission System Operator's (TSO) demand.

#### A. Scenario analysis and time-series prediction

One of the main issues in the decision-making of power systems is how to estimate the uncertainty and variability nature of wind power and how this variability can be incorporated into optimization modeling. The bidding decision variables in the day-ahead market are selected based on possible wind speed scenarios and average expected grid frequency. However, in stochastic programming, the run-time highly depends on the number of scenarios. Therefore, an efficient scenario reduction approach is required to reduce the computational time required for simulating a large number of cases over a year. In [40], the advantages of incorporating a deep learning-based time-series forecasting method into a multistage stochastic programming framework are discussed. Fig. 6 shows, the Group Method of Data Handling (GMDH) is used as a deep learning method to estimate the likelihood of four wind scenarios, which their occurrence has a major impact on the bidding strategy. The GMDH employs a combination of quadratic and higher polynomial functions in a particular number of layers and maps input features to the expected output by creating a multistage nonlinear pattern [41]. In this study, the GMDH is mainly used as a prediction tool to forecast time series of wind speed and grid frequency. The structure of the GMDH network can be created automatically, only based on prepared training and testing data sets. Moreover, the GMDH is a self-organizing algorithm that

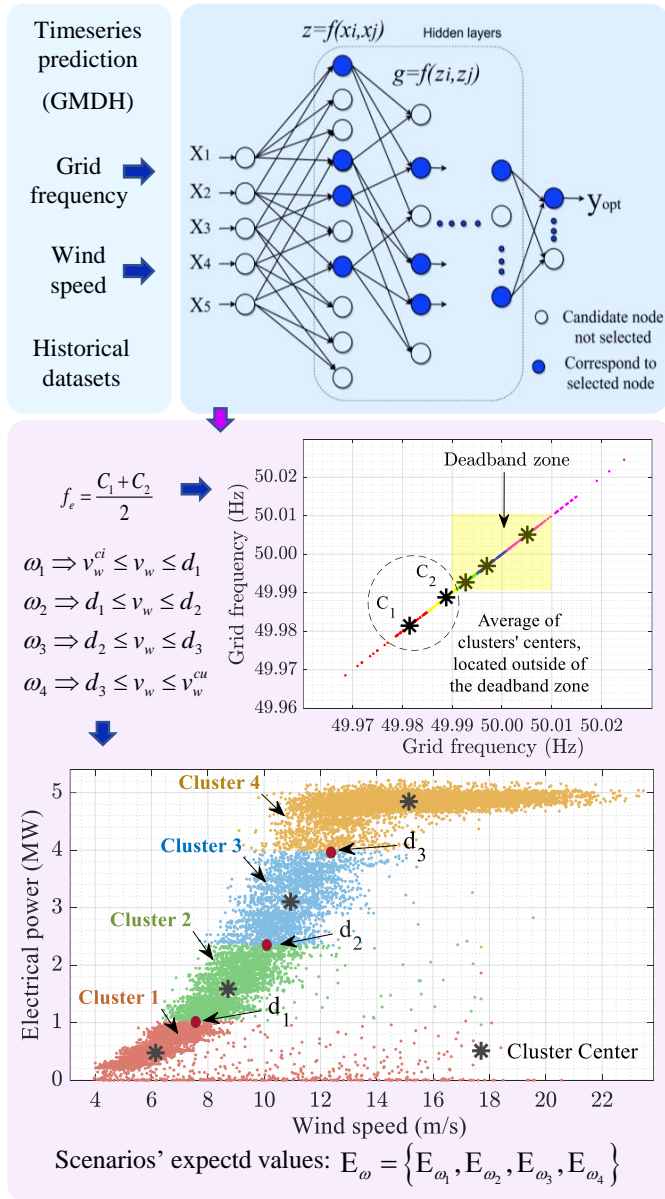


Figure 6: Estimating expected value of each scenario based on day-ahead predictions of wind speed and grid frequency.

gradually sorts out complicated polynomial models and selects the best solution using the external criterion. Hence, it usually needs less training data to overcome the prediction problem. As mentioned, reducing the number of scenarios representing the underlying uncertainty is often essential to finding efficient numerical solutions. Finding a smaller subset of scenarios reduces the numerical complexity while keeping the error at an acceptable level. Therefore, a computationally efficient methodology is used to tackle the scenario reduction problem. A clustering method based on the K-means algorithm is used to partition the scenario sets. Each cluster represents the scenario that best mirrors the conditional objective values for that specific operational condition. Four scenarios are foreseen based on the wind speed distribution to cover all the wind turbine operating regions gradually. The wind speed is above the rated value in the fourth scenario  $\omega_4$ . Therefore, the surplus power is consumed by the formic acid plant, which

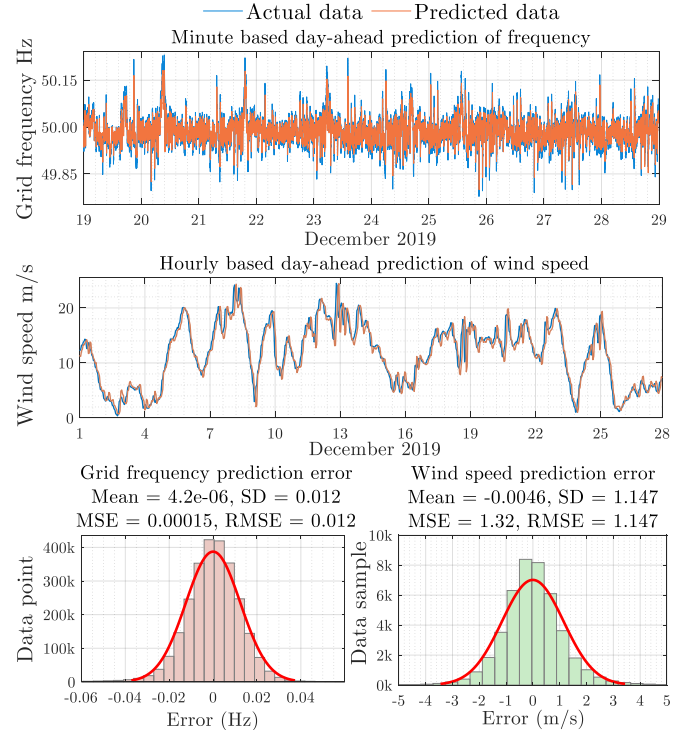


Figure 7: Wind speed and grid frequency day-ahead prediction.

results in further CO<sub>2</sub> capture. In the first scenario  $\omega_1$ , wind power is less than half of the maximum capacity of the chemical process. In the second and third scenarios  $\omega_2$  and  $\omega_3$ , the wind speed is below the rated value and above the maximum capacity of the chemical process. Furthermore, the grid frequency situation can be determined by estimating the mean frequency on a quarter-hourly basis depending on the TSO's penalty mechanism. The K-means algorithm is also used for finding the grid frequency mean value considering the density of data points located below or above nominal frequency. Fig 6 shows an example of the grid frequency that seems to be occurring below the nominal value, where the average of the central clusters outside the dead-band zone is 49.985 Hz. Fig 7 also reveals the results of the wind speed and grid frequency prediction using historical datasets over five years, i.e., from January 2015 till December 2019. The Mean, Root Mean Square Error (RMSE), Mean Square Error (MSE), and Standard Deviation (SD) of the absolute errors are the evaluation metrics used for assessing the results.

### B. Stochastic optimization

The bidding decision variables of electricity  $P_e^{sch}$  and reserve  $P_r^{sch}$  are defined as first-stage decision variables. These should be scheduled in the day-ahead market. The decision variables related to formic acid production  $p_{Fa}^{sch}$ , electricity and reserve commitments,  $P_e(\omega)$  and  $P_r(\omega)$  respectively, are defined as second-stage variables. The decision-maker does not need to select the formic acid production schedule in the day-ahead but can take advantage of the plant's flexibility to optimize the baseload of formic acid production  $p_{Fa}(\omega)$  according to the different wind speed scenarios that may occur. Therefore, the two-stage stochastic optimization model and its

constraints are formulated, based on the above considerations, as follows:

$$\max \left[ \begin{array}{l} (P_e^{\text{sch}} \cdot \lambda_e^{\text{sch}} + P_r^{\text{sch}} \cdot \lambda_r^{\text{sch}}) \cdot \Delta T + \\ \mathbb{E}_\omega \left( g(p_{\text{Fa}}(\omega)) \cdot \lambda_{\text{Fa}} + \right. \\ \left. (\Delta P_e(\omega) \cdot \lambda_{\Delta e} + \Delta P_r(\omega) \cdot \lambda_{\Delta r}) \cdot \Delta T \right) \end{array} \right] \quad (11)$$

$$\Delta P_e(\omega) \cdot \lambda_{\Delta e} = \Delta P_e^+(\omega) \cdot \lambda_{\Delta e}^+ - \Delta P_e^-(\omega) \cdot \lambda_{\Delta e}^- \quad (12)$$

$$P_\omega = 2 \cdot P_{\text{wt}} \quad (13)$$

$$\Delta P_r(\omega) \cdot \lambda_{\Delta r} = \Delta P_r^+(\omega) \cdot \lambda_{\Delta r}^+ - \Delta P_r^-(\omega) \cdot \lambda_{\Delta r}^- \quad (14)$$

$$P_r^{\text{sch}} = 200\text{mHz} \cdot K \quad (K \text{ is droop constant}) \quad (15)$$

$$P_r(\omega) = \Delta f \cdot K \quad (16)$$

$$\Delta f = f_e - f_{\text{ref}} \quad (f_{\text{ref}} \text{ is } 50 \text{ Hz}) \quad (17)$$

where  $\lambda_e^{\text{sch}}$ ,  $\lambda_r^{\text{sch}}$  and  $\lambda_{\text{Fa}}$  are the electricity, reserve and formic acid prices respectively.  $\mathbb{E}_\omega$  is the probability of scenario  $\omega$ .  $\Delta P_e^+(\omega)$ ,  $\Delta P_e^-(\omega)$ ,  $\Delta P_r^+(\omega)$  and  $\Delta P_r^-(\omega)$  are additional and deficiency of power injection to the grid and reserve provision.  $\lambda_{\Delta e}^-$ ,  $\lambda_{\Delta e}^+$ ,  $\lambda_{\Delta r}^-$  and  $\lambda_{\Delta r}^+$  are revenue and penalty for additional power and reserve injected to the grid as well. The optimization will be carried out for 24 hours considering market parameters with quarter-hourly basis.  $\Delta T$  is the time interval for electricity injection and frequency regulation, i.e. 15 minutes. The TSO has different mechanisms to penalize electricity and reserve providers if they violate their scheduled electricity and reserve contributions based on the contracted agreement. In this study, it has been assumed that electricity production can be addressed in the framework of a Balance Responsible Party (BRP). Therefore, the imbalance in energy settlement takes place in real-time on a quarter-hourly basis. Consequently, the energy provider gets a reduced revenue and penalty for its positive and negative deviation at each settlement course when the generated power is higher than the scheduled power as follows:

$$\lambda_{\Delta e}^+ = \lambda_e^{\text{sch}} - \alpha \quad (18)$$

$$\lambda_{\Delta e}^- = \lambda_e^{\text{sch}} + \alpha \quad (19)$$

where  $\alpha$  is an additional incentive component, which depends on the average of the absolute values of the System Imbalance (SI) of the current and the previous imbalance settlement period.  $\alpha$  can be expressed by an S-shaped curve that rises rapidly until 200 €/MWh and then saturates at the maximum value of 200 €/MWh [42]. Moreover, based on the Balancing Service Provider (BSP) contract, the BSP must activate automatically (without intervention) the FCR Requested with the penalties for FCR missing MW on a quarter-hourly basis as follows:

$$\lambda_{\Delta r}^- = 0.2 \cdot \beta \cdot \lambda_r^{\text{M}}; \quad \lambda_{\Delta r}^+ = 0 \quad (20)$$

$$\beta = \frac{P_r^{\text{sch}} - P_r}{P_r^{\text{sch}}} \quad (21)$$

where  $\beta$  is the failure factor, which increases by the difference between the scheduled FCR and the activated one, i.e.  $P_r$ .  $\lambda_r^{\text{M}}$  is the total remuneration for the FCR awarded for month M [43]. Also, the penalty of missing time for FCR

provision (delaying in reserve activation) can be calculated on a monthly basis. However, this penalty is not considered in this optimization problem as the proposed control system acts immediately to the frequency deviations (varying every 10 s) and does not technically/intentionally postpone the FCR activation.

In the first and second stage of the optimization, the objective function (11) is subject to the following boundary conditions:

s.t. (first stage)

$$0 \leq P_e^{\text{sch}} \leq P_\omega^{\text{max}} \quad (22)$$

$$0 \leq P_r^{\text{sch}} \leq \frac{P_{\text{Fa}}^{\text{max}} - P_{\text{Fa}}^{\text{min}}}{2} \quad (23)$$

The constraint (22) limits the contribution of electricity to the available wind energy. The constraint (23) restricts the symmetric upward and downward scheduled power reserve to the formic acid minimum and maximum capacity (i) to guarantee the continuous operation of the electrolyzer, and (ii) to avoid any start-up and shut-down time required to purge the nitrogen.

s.t. (second stage)

$$P_{\text{Fa}}^{\text{min}} \leq P_{\text{Fa}}^{\text{opr}}(\omega) \leq P_\omega \quad (24)$$

$$P_{\text{Fa}}^{\text{opr}} = P_\omega - P_e(\omega) - P_r(\omega) \quad \text{if } 49.8 \leq f_e \leq 49.99 \quad (25)$$

$$P_{\text{Fa}}^{\text{opr}} = P_\omega - P_e(\omega) + P_r(\omega) \quad \text{if } 50.01 \leq f_e \leq 50.2 \quad (26)$$

$$0 \leq P_e(\omega) \leq P_\omega - p_{\text{Fa}}(\omega) \quad (27)$$

$$0 \leq P_r(\omega) \leq \frac{p_{\text{Fa}}(\omega)}{2} \quad (28)$$

$$\Delta P_e^+(\omega) = P_e(\omega) - P_e^{\text{sch}} \quad \text{if } P_e(\omega) > P_e^{\text{sch}} \quad (29)$$

$$\Delta P_r^+(\omega) = P_r(\omega) - P_r^{\text{sch}} \cdot \Delta f \quad \text{if } P_r(\omega) > P_r^{\text{sch}} \quad (30)$$

$$\Delta P_e^-(\omega) = P_e(\omega) - P_e^{\text{sch}} \quad \text{if } P_e(\omega) \leq P_e^{\text{sch}} \quad (31)$$

$$\Delta P_r^-(\omega) = P_r(\omega) - P_r^{\text{sch}} \cdot \Delta f \quad \text{if } P_r(\omega) \leq P_r^{\text{sch}} \quad (32)$$

the nonlinear functions  $P_{\text{wt}}$  and  $P_{\text{Fa}}^{\text{opr}}(\omega)$  and their piecewise linearizations are given in (9), (10), (5) and (6), which are discussed in detail in § II-B and § II-A. The constraint (24) avoids exceeding the minimum capacity of the plant and the total available power with the formic acid production. The constraints (25) and (26) define upward and downward regulations when the grid frequency drops or goes above 50 Hz, considering the deadband zone. The constraints (27) and (28) are the limitations for electricity injection and reserve activation. The constraints (29) to (32) are considered for penalizing the electricity extra injection/off-takes and over/under reserve activations based on what was scheduled.



### C. Mixed-integer nonlinear programming problem

It is essential to adopt nonlinear terms to capture specific operational characteristics of the chemical plant in formulating the optimization problem. Nevertheless, using nonlinear terms generally increases computational complexity and time, which motivates the development of efficient transformation and linearization approaches. Such linearizations are expected to decrease the computational complexity and facilitate decision-making.

The proposed two-stage stochastic optimization is solved using mixed-integer nonlinear programming (MINLP). Both the nonlinear function of formic acid (5) and its piecewise form (6) are considered to investigate the reliability and computational efficiency of the proposed problem. It is important to note that binary integer variables used in this problem formulating the upward and downward regulations are inherently nonconvex. However, the MINLP solver used in this study combines constraint propagation and interval analysis and takes advantage of the enhanced branch and bound concept for the quadratic objective function to handle any non-convexity in its search for globally optimal solutions [44]. Furthermore, fitting a convex piecewise linear function guarantees finding feasible solutions for the corresponding original convex nonlinear subproblem [44]. Accordingly, adding more nodes or segments challenges neither the convex optimization nor finding the global optimum but instead increases the accuracy of the nonlinear approximation and the computational load [45].

In this study, the applied MINLP solver operates based on a polyhedral branch and bound technique, advanced bound tightening as well as range reduction strategies to reduce the search space. It employs local search techniques as primal heuristics. Moreover, as a standard and widely-used metric for evaluating approaches that solve combinational optimization problems, the optimality gap is estimated. This index, which gives the relative and absolute distance between an approximate solution and the optimal solution, is estimated for nonlinear and piecewise models. The relative and absolute gaps for the nonlinear function are  $9.9 \times 10^{-10}$  and  $9.4 \times 10^{-7}$ , respectively. The same parameters for the piecewise function are  $4.5 \times 10^{-13}$  and  $4.2 \times 10^{-10}$ , respectively, which shows the effectiveness of the proposed models for finding the optimum.

## IV. RESULTS

### A. The impact of variable wind power on decision making

One of the most critical issues with the bidding strategies of the flexible demand, integrated with renewable sources, is the trade-off between the power consumption and the injection of additional renewable power into the grid. If the decision-maker offers a too high bidding quantity, it will not satisfy grid requirements in low wind power scenarios. It will be subject to penalties, leading to an additional cost. However, a low bidding quantity of reserve and electricity causes extra wind power curtailment and declines revenue. Hence, the optimization criteria proposed in this study guarantee an offer which is a compromise between an aggressive decision with a high bidding quantity and a conservative decision with a low bidding quantity, considering the variability of wind

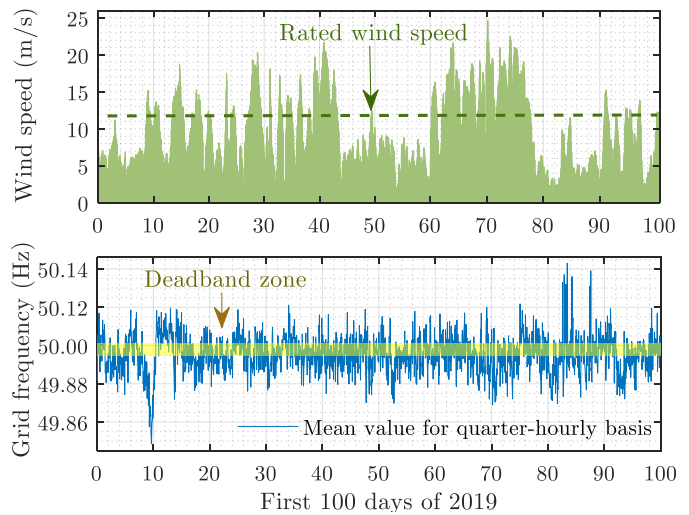


Figure 8: Wind and grid frequency profile for the first 100 days of 2019.

and grid frequency. Table I gives the optimal allocation of available wind power to the electricity/reserve markets and the formic acid production for the proposed and baseline strategies. No operational flexibility and FCR provision are considered for the baseline approach, and the available wind power is only decided to be optimally distributed between the chemical process and the electricity market. It can be understood that the proposed strategy suggests almost zero contribution to the electricity market on an almost windless day when the wind speed is too low. However, a marginal reserve contribution is decided since the maximum frequency deviation rises to 50.122 Hz, and the chemical process can play a demand response role in consuming excessive supplied power. Instead, any available wind speed will be allocated to formic acid production. Thus, there will be a minimum formic acid production even in the first scenario  $\omega_1$  when the average estimated frequency exceeds 50 Hz. This condition does not happen so often due to some degree of correlation between wind speed and grid frequency. Nevertheless, for the following case, i.e. an almost windless day with a wind speed between 3 and 6 m/s and a maximum frequency deviation of 49.948 Hz, no reserve is arranged to avoid activation penalties for the windless condition. Contrarily, a maximum contribution in electricity and reserve markets will be selected for windy and extremely windy days. According to Table I, the results of the proposed optimization problem for an extremely windy day show an almost equal amount of bids for both scheduled electricity and reserve. The average wind speed is above the rated value on a windy day, but it may also drop for a meaningful period. Therefore, a higher contribution to the electricity market is suggested to avoid extra penalties of the reserve that will be asked for activation, especially when the maximum estimated grid frequency is below 50 Hz. An even more conservative policy is taken for the day, meeting variable wind conditions. The results show that the proposed strategy effectively prioritizes formic acid production based on available wind power over all the scenarios, and actively participates in the reserve and electricity market to enhance the income  $Z$  given by (11). At the same time, the baseline

Table I: Optimal decision for the proposed and baseline strategies in different days, various wind and frequency conditions.

Days of 2019	Operation mode	$P_e^{sch}$	$P_r^{sch}$	$f_e$	$P_{Fa}^{OPF}(\omega)$ (MW)				$Z, Z_b$
		day a head schedule	schedule	Hz	$\omega_1$	$\omega_2$	$\omega_3$	$\omega_4$	euro
Almost windless: $v_w \leq 4$ m/s	Proposed strategy	0	0.33		0.44	1.48	4.00	0	173.68
	Baseline approach	0	No FCR	50.122	0.44	1.47	4.00	0	138.94
Windless: $3 \text{ m/s} \leq v_w \leq 6 \text{ m/s}$	Proposed strategy	0.86	0		0	2.16	4.95	0	504.57
	Baseline approach	1.31	No FCR	49.948	0	2.15	4.53	0	408.91
Variable wind: $5 \text{ m/s} \leq v_w \leq 25 \text{ m/s}$	Proposed strategy	4.68	0.50		0.57	2.99	4.61	4.92	730.25
	Baseline approach	5.54	No FCR	50.101	0.57	1.49	4.06	4.45	617.47
Windy: $v_w \geq 10 \text{ m/s}$	Proposed strategy	4.14	1.01		0	2.02	4.61	4.84	910.43
	Baseline approach	5.64	No FCR	49.921	0	3.03	4.06	4.35	768.22
Extremely windy: $v_w \geq 12 \text{ m/s}$	Proposed strategy	2.26	2.58		0	0	5.16	5.16	1041.70
	Baseline approach	5.62	No FCR	49.916	0	0	4.12	4.38	874.511

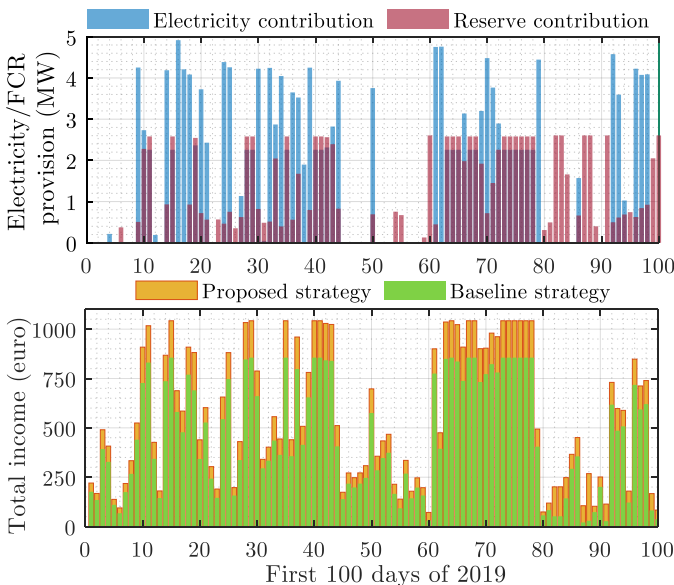


Figure 9: The two-stage stochastic programming performance for the first 100 days of 2019.

approach only guarantees the optimal base-load of formic acid production and relatively increases the electricity market share by rising wind speed up to the rated power (10 MW).

Fig. 8 shows the wind and grid frequency variations for the first 100 days of 2019. Fig. 9 also shows the performance of the two-stage stochastic programming for the same wind and frequency situation when the prices mentioned above are competitive, and the decision maker is willing to participate in all the markets. It shows that whenever the wind speed is above the rated value (11.9 m/s), the maximum reserve bidding quantity is decided, which is half of the maximum capacity of the formic acid process, around 2.60 MW, to satisfy the symmetric (upward and downward) FCR. However, the priority is to produce formic acid when wind speed is expected to drop significantly. For the expected unstable wind and variable frequency conditions, the preference is to offer a higher electricity contribution to avoid FCR penalties in low wind speed events. Also, in Fig. 9, the total income considering the proposed operational strategy is compared with the baseline strategy, where no flexibility and reserve contribution is supported, and the wind power is only allocated to the chemical process and the electricity market. The average revenue is increased for the proposed strategy compared to the baseline approach as a result of the offered flexibility and FCR provision, especially in above-rated wind speeds.

### B. Economic efficiency

Although the primary goal of the proposed two-stage stochastic programming is to deal with wind power uncertainty, the optimization's parameters are set to obtain the maximum sensitivity to electricity, reserve and formic acid prices. Fig. 10 compares the economic efficiency of the proposed model for two pricing conditions with the same wind and grid frequency profiles shown in Fig. 8. First, when the reserve price is much lower than the electricity price ( $\lambda_r^{sch} \ll \lambda_e^{sch}$ ) and second, when the reserve price is competitive to the electricity price ( $\lambda_r^{sch} \geq \lambda_e^{sch}$ ). The first pricing condition represents the lowest reserve price according to market prices in 2019, and the second pricing condition is more likely to happen in the future of power systems without conventional plants. It can be witnessed that in the first pricing condition, lower economic efficiency is achieved because the stochastic programming does not suggest contribution to the reserve market, except for a couple of days, i.e. between days 80 and 90, where the grid frequency is foreseen to go above 50 Hz. The economic efficiency improvement EE is defined by:

$$EE = \frac{Z(\lambda_r^{sch} \gg \lambda_e^{sch}) - Z(\lambda_r^{sch} \ll \lambda_e^{sch})}{Z_b} \times 100 \quad (33)$$

where  $Z_b$  is the calculated income for a baseload operational strategy. The estimation of EE shows the degree of freedom of the decision-maker and explains up to what level he contributes to the reserve market based on reserve prices.

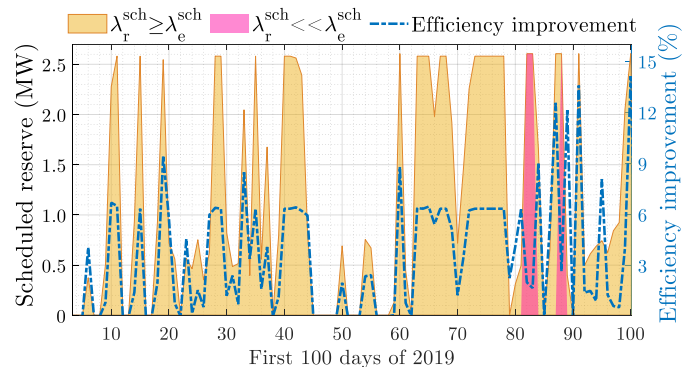


Figure 10: Economic efficiency (right axis in percentage) considering two optimal scheduled reserve quantities (left axis in MW) with two pricing scenarios (yellow and pink).

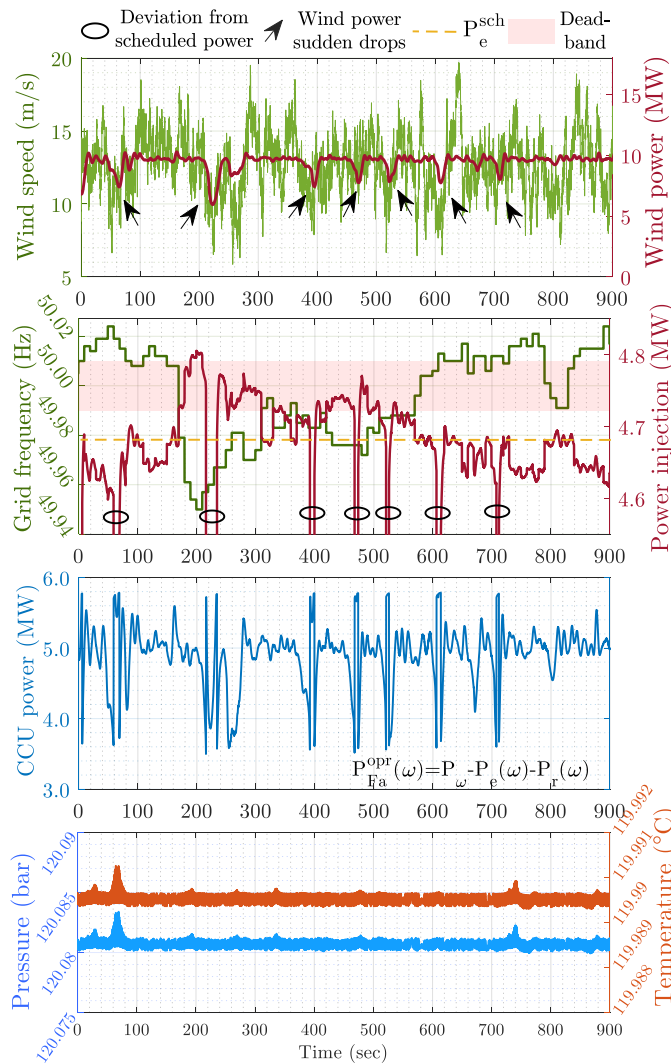


Figure 11: Dynamic performance under varying wind conditions and grid frequency changes. Figures from top to bottom illustrate wind and frequency profiles,  $P_g(\omega)$  total injected electricity and reserve power to the grid, power consumption of the CCU plant, and the reactor inlet pressure and temperature.

### C. Dynamic performance analysis

The performance of the proposed control scheme needs to be evaluated in extreme cases to ensure the reliability and efficiency of the proposed operational strategy. Therefore, a dynamic simulation is carried out in varying wind conditions between 4 to 20 m/s with significant turbulence (>17%). Also, the used grid frequency profile contains data points both above and below 50 Hz, and requests upward and downward FCR for 900 s. Fig. 11 shows the dynamic simulation results, including the sum of the injected power to the grid (electricity and reserve activation) and the chemical plant operating power with the reactor inlet pressure and temperature. Although an extremely variable wind speed profile is considered, which drops to very low wind speeds rapidly, the proposed control system is able to regulate the compressors rotational speed, the reactor inlet temperature and the pressure. Also, it keeps the power consumption in the recommended range of 3 to

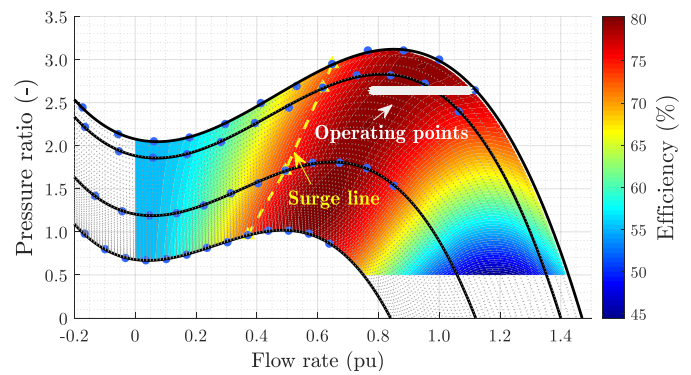


Figure 12: The compressor performance at the CO<sub>2</sub> compression stage on the efficiency map.

5.7 MW. The proposed stochastic programming schedules the contribution of 4.68 MW and 0.5 MW to the electricity and reserve markets for such wind and frequency scenarios. However, there will be deviations from the scheduled power (maximum deviation is 1.57 MW) due to insufficient available wind power, which is inevitable but still economically feasible based on the penalty mechanism. If the TSO considers higher penalties for less severe violations, the stochastic programming offers lower contributions to avoid extreme deviations accordingly.

Fig. 12 also illustrates the compressor's dynamic performance at the CO<sub>2</sub> compression stage. The first compressor in the CO<sub>2</sub> stream is responsible for adjusting the CO<sub>2</sub> flow rate such that the required CO<sub>2</sub>/H<sub>2</sub> ratio is maintained at the reactor while supplying the desired discharge pressure. As indicated, the CO<sub>2</sub> and H<sub>2</sub> flow rate ratio is kept consistent at the desired level, and the discharge pressure is maintained at a nearly constant level despite the variations in hydrogen production. Surge and stall operation are actively avoided by the control algorithm. The other four compressors follow the first compressor discharge flow rate to ensure the output pressures will be at the permitted level. It is also recommended that the compressors' sizing should be appropriately determined by the equipment sizing in the planning phase, ensuring high efficiency for the expected varying operational conditions.

Both the proposed control systems and the optimization algorithm contain means to ensure safe operation, i.e., saturation of signals within safe limits, rate limiters to avoid extreme dynamics, and boundary conditions in the optimization. Upon practical implementation, these can all be configured to ensure safe operation. Nevertheless, the mentioned limitations and dynamic behaviour of the reactor need to be considered in the equipment sizing and/or an auxiliary storage tank can be required.

## V. CONCLUSIONS

In this study, a two-stage stochastic programming model considering wind power uncertainty is employed to investigate an optimal Collaborative flexible operation of a CCU-based chemical process as an energy-intensive industrial load with wind power. Although demand and renewable sources are envisioned to play an essential role in the ancillary market, offering grid balancing services in a collaborative procedure

is not yet well explored. Therefore, this paper suggests a decision-making algorithm, which guarantees an optimal bidding strategy for the hybrid system consisting of a CCU-based process and two wind turbines, participating in the day-ahead electricity and reserve markets. The dynamic modeling of the subsystems and the proposed architecture of the chemical plant are presented in detail, and their piecewise linearization is used in the optimization algorithm. The proposed algorithm is not limited by period spans and can be applied to other markets as well, e.g., the intra-day market. Instead of generating hundreds of scenarios that can make the optimization computationally expensive, the GMDH algorithm is used as a deep learning time-series prediction tool for forecasting wind speed and grid frequency in a day ahead. Accordingly, four wind scenarios are considered that can particularly impact the optimal bidding strategy. The results show the significance of the proposed stochastic programming to find an optimal decision for the bidding strategy and the formic acid production. This approach ensures sufficient carbon-dioxide capture and an optimal provision of FCR as vital elements towards decarbonizing the grid.

#### ACKNOWLEDGMENT

This research is part of the Catalisti cluster SBO project CO2PERATE with the financial support of VLAIO (Flemish Agency for Innovation and Entrepreneurship), and the Energy Transition Fund (ETF) project BEOWind funded by the Belgian federal government.

#### REFERENCES

- [1] H. L. van Soest, M. G. den Elzen, and D. P. van Vuuren, "Net-zero emission targets for major emitting countries consistent with the Paris Agreement," *Nature Communications*, vol. 12, no. 1, pp. 1–9, 2021.
- [2] L. Haar, "An empirical analysis of the fiscal incidence of renewable energy support in the European Union," *Energy Policy*, vol. 143, p. 111483, 2020.
- [3] I. Pineda, "Aiming high—rewarding ambition in wind energy," *A position paper by the European Wind Energy Association*, 2015.
- [4] C. Schwarte, "EU climate policy under the Paris Agreement," *Climate Law*, vol. 11, no. 2, pp. 157–175, 2021.
- [5] M. Rosental, T. Fröhlich, and A. Liebich, "Life cycle assessment of carbon capture and utilization for the production of large volume organic chemicals," *Frontiers in Climate*, vol. 2, p. 9, 2020.
- [6] Z. Sun, L. Zeng, C. K. Russell, S. Assabumrungrat, S. Chen, L. Duan, W. Xiang, and J. Gong, "Solar–wind–bio ecosystem for biomass cascade utilization with multigeneration of formic acid, hydrogen, and graphene," *ACS Sustainable Chemistry & Engineering*, vol. 7, no. 2, pp. 2558–2568, 2018.
- [7] D. Ravikumar, G. Keoleian, and S. Miller, "The environmental opportunity cost of using renewable energy for carbon capture and utilization for methanol production," *Applied Energy*, vol. 279, p. 115770, 2020.
- [8] B. Lee, H. Lee, D. Lim, B. Brigljević, W. Cho, H.-S. Cho, C.-H. Kim, and H. Lim, "Renewable methanol synthesis from renewable H<sub>2</sub> and captured CO<sub>2</sub>: How can power-to-liquid technology be economically feasible?" *Applied Energy*, vol. 279, p. 115827, 2020.
- [9] H. Saboori and R. Hemmati, "Considering carbon capture and storage in electricity generation expansion planning," *IEEE Transactions on Sustainable Energy*, vol. 7, no. 4, pp. 1371–1378, 2016.
- [10] A. I. Osman, M. Hefny, M. A. Maksoud, A. M. Elgarahy, and D. W. Rooney, "Recent advances in carbon capture storage and utilisation technologies: a review," *Environmental Chemistry Letters*, pp. 1–53, 2020.
- [11] M. Bos, S. Kersten, and D. Brilman, "Wind power to methanol: Renewable methanol production using electricity, electrolysis of water and CO<sub>2</sub> air capture," *Applied Energy*, vol. 264, p. 114672, 2020.
- [12] C. Chen and A. Yang, "Power-to-methanol: The role of process flexibility in the integration of variable renewable energy into chemical production," *Energy Conversion and Management*, vol. 228, p. 113673, 2021.
- [13] C. Hank, S. Gelpke, A. Schnabl, R. J. White, J. Full, N. Wiebe, T. Smolinka, A. Schaadt, H.-M. Henning, and C. Hebling, "Economics & carbon dioxide avoidance cost of methanol production based on renewable hydrogen and recycled carbon dioxide—power-to-methanol," *Sustainable Energy & Fuels*, vol. 2, no. 6, pp. 1244–1261, 2018.
- [14] N. Li, X. Zhao, X. Shi, Z. Pei, H. Mu, and F. Taghizadeh-Hesary, "Integrated energy systems with CCHP and hydrogen supply: A new outlet for curtailed wind power," *Applied Energy*, vol. 303, p. 117619, 2021.
- [15] M. Martín, "Methodology for solar and wind energy chemical storage facilities design under uncertainty: Methanol production from CO<sub>2</sub> and hydrogen," *Computers & Chemical Engineering*, vol. 92, pp. 43–54, 2016.
- [16] M. Martín and I. E. Grossmann, "Optimal integration of renewable based processes for fuels and power production: Spain case study," *Applied Energy*, vol. 213, pp. 595–610, 2018.
- [17] A. E. Samani, J. D. M. De Kooning, C. A. Urbina Blanco, and L. Vandevelde, "Flexible operation strategy for formic acid synthesis providing frequency containment reserve in smart grids," *International Journal of Electrical Power & Energy Systems*, vol. 139, p. 107969, 2022, DOI: 10.1016/j.ijepes.2022.107969.
- [18] I. González-Aparicio, Z. Kapetaki, and E. Tzimas, "Wind energy and carbon dioxide utilisation as an alternative business model for energy producers: A case study in Spain," *Applied Energy*, vol. 222, pp. 216–227, 2018.
- [19] O. Babatunde, J. Munda, and Y. Hamam, "Power system flexibility: A review," *Energy Reports*, vol. 6, pp. 101–106, 2020.
- [20] J. Zhao, T. Zheng, and E. Litvinov, "A unified framework for defining and measuring flexibility in power system," *IEEE Transactions on Power Systems*, vol. 31, no. 1, pp. 339–347, 2015.
- [21] M. Melliger and E. Chappin, "Phasing out support schemes for renewables in neighbouring countries: An agent-based model with investment preferences," *Applied Energy*, vol. 305, p. 117959, 2022.
- [22] H. Liu, P. Zeng, J. Guo, H. Wu, and S. Ge, "An optimization strategy of controlled electric vehicle charging considering demand side response and regional wind and photovoltaic," *Journal of Modern Power Systems and Clean Energy*, vol. 3, no. 2, pp. 232–239, 2015.
- [23] J. Wu, B. Zhang, Y. Jiang, P. Bie, and H. Li, "Chance-constrained stochastic congestion management of power systems considering uncertainty of wind power and demand side response," *International Journal of Electrical Power & Energy Systems*, vol. 107, pp. 703–714, 2019.
- [24] S. Cui, Y.-W. Wang, J.-W. Xiao, and N. Liu, "A two-stage robust energy sharing management for prosumer microgrid," *IEEE Transactions on Industrial Informatics*, vol. 15, no. 5, pp. 2741–2752, 2018.
- [25] M. Andérez-Fernández, E. Pérez, S. Ferrero, C. M. Álvarez, J. Gumiel, Ángel Martín, and M. D. Bermejo, "Simultaneous formic acid production by hydrothermal CO<sub>2</sub> reduction and biomass derivatives conversion in a continuous reactor," *Chemical Engineering Journal*, vol. 453, p. 139741, 2023. [Online]. Available: <https://www.sciencedirect.com/science/article/pii/S1385894722052202>
- [26] A. W. Dowling and V. M. Zavala, "Economic opportunities for industrial systems from frequency regulation markets," *Computers and Chemical Engineering*, vol. 114, pp. 254–264, 2018, fOCAPO/CPC 2017. [Online]. Available: <https://www.sciencedirect.com/science/article/pii/S009813541730323X>
- [27] "Establishing a guideline on electricity transmission system operation," 2017, URL: <https://eur-lex.europa.eu/>.
- [28] K. Lebling, H. Leslie-Bole, Z. Byrum, and E. Bridgwater, 6 things to know about direct air capture. [Online]. Available: <https://www.wri.org/insights/direct-air-capture-resource-considerations-and-costs-carbon-removal>
- [29] K. Park, G. H. Gunasekar, S.-H. Kim, H. Park, S. Kim, K. Park, K.-D. Jung, and S. Yoon, "CO<sub>2</sub> hydrogenation to formic acid over heterogenized ruthenium catalysts using a fixed bed reactor with separation units," *Green Chemistry*, vol. 22, no. 5, pp. 1639–1649, 2020.
- [30] Q. Wang, S. Santos, C. A. Urbina-Blanco, W. Y. Hernández, M. Impérator-Clerc, E. I. Vovk, M. Marinova, O. Ersen, W. Baaziz, O. V. Safonova *et al.*, "Solid micellar Ru single-atom catalysts for the water-free hydrogenation of CO<sub>2</sub> to formic acid," *Applied Catalysis B: Environmental*, vol. 290, p. 120036, 2021, DOI: 10.1016/j.apcatb.2021.120036.
- [31] J. J. Anderson, D. J. Drury, J. E. Hamlin, and A. G. Kent, "Process for the preparation of formic acid," 2019,

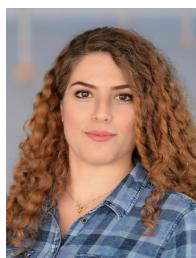
URL: <https://patentscope.wipo.int/search/en/detail.jsf?docId=WO19860-02066>.

- [32] J. D. M. De Kooning, J. Van de Vyver, B. Meersman, and L. Vandevelde, "Maximum efficiency current waveforms for a PMSM including iron losses and armature reaction," *IEEE Transactions on Industry Applications*, vol. 53, no. 4, pp. 3336–3344, 2017.
- [33] E. Giglio, R. Pirone, and S. Bensaid, "Dynamic modelling of methanation reactors during start-up and regulation in intermittent power-to-gas applications," *Renewable Energy*, vol. 170, pp. 1040–1051, 2021.
- [34] C. Dannesboe, J. B. Hansen, and I. Johannsen, "Catalytic methanation of CO<sub>2</sub> in biogas: Experimental results from a reactor at full scale," *Reaction Chemistry & Engineering*, vol. 5, no. 1, pp. 183–189, 2020.
- [35] S. Chatterjee, I. Dutta, Y. Lum, Z. Lai, and K.-W. Huang, "Enabling storage and utilization of low-carbon electricity: power to formic acid," *Energy & Environmental Science*, vol. 14, no. 3, pp. 1194–1246, 2021.
- [36] J. Jonkman, S. Butterfield, W. Musial, and G. Scott, "Definition of a 5-MW reference wind turbine for offshore system development," National Renewable Energy Lab (NREL), Golden, CO (United States), Tech. Rep., 2009.
- [37] J. D. M. De Kooning, T. L. Vandoorn, J. Van de Vyver, B. Meersman, and L. Vandevelde, "Displacement of the maximum power point caused by losses in wind turbine systems," *Renewable Energy*, vol. 85, pp. 273–280, 2016.
- [38] N. Kayedpour, A. E. Samani, J. D. M. De Kooning, L. Vandevelde, and G. Crevecoeur, "Model predictive control with a cascaded hamsterstein neural network of a wind turbine providing frequency containment reserve," *IEEE Transactions on Energy Conversion*, 2021.
- [39] A. E. Samani, J. D. M. De Kooning, N. Kayedpour, N. Singh, and L. Vandevelde, "The impact of pitch-to-stall and pitch-to-feather control on the structural loads and the pitch mechanism of a wind turbine," *Energies*, vol. 13, no. 17, p. 4503, 2020.
- [40] J. Wang, M. Cevik, and M. Bodur, "On the impact of deep learning-based time-series forecasts on multistage stochastic programming policies," *INFOR: Information Systems and Operational Research*, pp. 1–32, 2021.
- [41] N. Kayedpour, A. E. Samani, J. D. M. De Kooning, L. Vandevelde, and G. Crevecoeur, "A data-driven approach using deep learning time series prediction for forecasting power system variables," in *2019 IEEE 2nd International Conference on Renewable Energy and Power Engineering (REPE)*. Toronto, ON, Canada: IEEE, 2–4 Nov. 2019, pp. 43–47.
- [42] Elia. Day-ahead balance obligation of the balance responsible parties. [Online]. Available: <https://www.elia.be/en/public-consultation/20200922-public-consultation-on-day-ahead-balance-obligation-of-brps>
- [43] Elia. Terms and conditions for balancing service providers for frequency containment reserve (FCR). [Online]. Available: <https://www.elia.be/en/electricity-market-and-system-services/keeping-the-balance/fcrs>
- [44] T. Lastusilta, M. R. Bussieck, and T. Westerlund, "Comparison of some high-performance MINLP solvers," *Chem. Eng. Trans.*, vol. 11, pp. 125–130, 2007.
- [45] A. Inamoto and B. Tang, "A recursive descent algorithm for finding the optimal minimax piecewise linear approximation of convex functions," in *Advances in Electrical and Electronics Engineering-IAENG Special Edition of the World Congress on Engineering and Computer Science 2008*. IEEE, 2008, pp. 287–293.



**Arash E. Samani** (S'20) received his B.S. degree in mechanical engineering from IAU University in Isfahan, Iran, in 2011, and his M.S. degree in mechanical engineering from Politecnico di Milano in Milan, Italy, in 2016. He completed his Ph.D. studies in electromechanical engineering at Ghent University in Belgium in 2022. He has conducted research in wind turbine performance analysis, aerodynamic modelling, and structural load analysis. He is currently engaged in research aimed at developing a novel approach to enhance the flexibility of

power systems. His research seeks to facilitate the integration of renewables into power systems, thereby supporting the transition towards a low-carbon paradigm.



**Nezmin Kayedpour** (S'20) received the B.Sc. degree in electrical engineering and M.Sc. in Mechatronics, Robotics, and Automation Engineering from QIAU, Iran, in 2016. She is currently working towards the Ph.D. degree in electromechanical engineering in the Electrical Energy Laboratory, Department of Electromechanical, Systems and Metal Engineering at Ghent University, Belgium. Her current research interests include renewable energy applications, fuzzy logic, advanced optimization and data-driven control in smart grids, model-based fault diagnosis for dynamic processes employing artificial intelligence and multi-criteria decision-making for the integration of wind farms. She is a member of the FlandersMake@UGent MIRO core lab.



**Farjam Kayedpour** received a B.S. degree in Industrial Management from Raja University, Qazvin, Iran, in 2009, and subsequently pursued M.S. and Ph.D. degrees in production and operations management from the Allameh Tabataba'i University, Tehran, Iran, in 2012 and 2021 respectively. During his academic career, he conducted research on designing resilient supply chains and optimizing reliability models. Currently, his research interests include optimization modeling under uncertainty, fuzzy and robust optimization, evolutionary algorithms, reliability engineering, and supply chain management.



**Jeroen D. M. De Kooning** (M'09, SM'20) was born in Kapellen, Belgium, in 1987. He received the Bachelor, Master and Ph.D. degrees in electromechanical engineering from Ghent University, Belgium, in 2008, 2010 and 2015 respectively. Since 2019, he is assistant professor at the Department of Electromechanical, Systems and Metal Engineering at the Faculty of Engineering and Architecture of Ghent University, Belgium. In 2022, he was a visiting professor at the Lappeenranta University of Technology, Finland. He is a member of the

Dynamical Systems and Control (DySC) research group and the Flanders-Make@UGent MIRO core lab. He conducted research on current waveform shaping techniques for permanent magnet synchronous machines, and optimal control and design of renewable energy systems. His present research interests include modelling, optimization and control of mechatronic systems, drivetrains and manufacturing machines in an Industry 4.0 context, with a particular interest in digital twins.



**Guillaume Crevecoeur** Guillaume Crevecoeur (°1981) received his Master and PhD degree in Engineering Physics from Ghent University in 2004 and 2009, respectively. He received a Research Foundation Flanders postdoctoral fellowship in 2009 and was appointed Associate Professor at Ghent University in 2014. He is member of Flanders Make in which he leads the Ghent University activities on machines, intelligence, robotics and control. With his team, he conducts research on system identification and nonlinear control for mechatronics, industrial robotics and energy systems. His goal is to endow physical dynamic systems with improved functionalities and capabilities when interacting with uncertain environments, other systems and humans.



**Lieven Vandevelde** (M'05, SM'07) was born in Eeklo, Belgium in 1968. He graduated in electrical & mechanical engineering (main subject: electrical power engineering) at Ghent University in 1992 and is since then with the Electrical Energy Laboratory (EELAB), Department of Electromechanical, Systems and Metal Engineering, Ghent University. He received the Ph.D. degree from Ghent University in 1997, and has conducted research in various domains of electrical power engineering, *inter alia* electrical machines and (computational) electromagnetics.

Since 2004, he has been member of the professorial staff and has been coordinating the research on electric power systems at EELAB. In this research, renewable energy and its integration in electric power systems play a prominent role.